NANO-SHORTS

Xiaojie Lou[1], Xiaobing Hu[2], Ming Zhang[1], S. A. T. Redfern[1], E.A. Kafadaryan[3] and J. F. Scott[1]

[1]Earth Sciences Department, University of Cambridge, Cambridge CB2 3EQ, U. K.
[2]Materials Science Department, University of Cambridge, Cambridge CB2 3EQ, U. K.
[3]Institute for Physical Research, NASA, Ashtarak-2, 378410, Armenia

Abstract. Micro-Raman and electron nano-probe techniques are used to show that lead zirconate-titanate (PZT) and samarium-doped bismuth titanate undergo local phase transformations during electrical shorting. In PZT dendrite-like shorts of a few microns diameter, produced by extreme bipolar voltage cycling fatigue, are mapped spectroscopically in 1 μm² areas and exhibit almost pure regions of α-PbO, β-PbO and rutile TiO_2. [Note that β-PbO is not the stable ambient phase.] Similarly, the Sm-doped bismuth titanate converts under large dc voltages from layered-perovskite structure to a pyrochlore-like structure during filamentary electrical breakdown, with the loss of Bi. The results complement the very recent hot luminescence study of J. C. Tsang and B. P. Lindner, Appl. Phys. Lett. **84** (2004) 4641 in related thin-film gate oxides.

1. INTRODUCTION

1.1. Breakdown kinetics

The process of electrical shorting in ferroelectric perovskite oxides such as lead zirconate titanate (PZT) was first shown by Plumlee [1] to arise from filamentary conduction pathways through the material, initiated at the anodes and/or cathodes. This mechanism was modelled in detail by Duiker *et al*. [2-4] in terms of oxygen-deficient pathways, however the chemical composition of the filaments was never analyzed spectroscopically until the present study.

To establish microscopic electrical mechanisms for breakdown in ferroelectric oxide films one must show that the dependences of breakdown field E_B upon film thickness d, area A, ramp rate $1/t_c$, temperature T, doping, and electrode metal are satisfied. The dependence for PZT upon film thickness is most compatible [5] with a low-power-law dependence or possibly logarithmic. The physical models compatible with this include avalanche (logarithmic), or collision ionization from electrons injected via field emission from the cathode, [6] which gives

$$E_B = A\, d^{-w} \tag{1}$$

with $1/4 < w < 1/2$, or the linked defect model, [7] which has $d = 0.39$.

The dependence on electrode material arises from the electrode work function and the ferroelectric electron affinity through the resultant Schottky barrier height. Following Von Hippel [8], we have [9]:

$$eE_B\lambda = h\,(\Phi_M - \Phi_{FE}), \tag{2}$$

where Φ_M and Φ_{FE} are the work functions of the metal and of the semiconducting ferroelectric; λ, the electron mean free path; and h, a constant of order unity. Typically [9] in Eq. (2) for oxide ferroelectrics

---

Corresponding author: X.J. Lou, email: XL217@cam.ac.uk

we have: E_B = 200-800 MV/m; the barrier height $(\Phi_M - \Phi_{FE})$ = 0.5 eV; and hence $\lambda = 1$ nm. It is important that λ is << the dimensions of the device considered (thickness d = 300-500 nm here) and also that $\lambda <$ the Schottky barrier width L at the electrode interface; this implies that there are no confinement energies in the problem and that the usual Schottky approximation, based upon $\lambda >> L$, is invalid.

In general electrical breakdown in ferroelectric oxides is a hybrid mechanism (like spark discharge in air) in which the initial phase is electrical but the final stage is simple thermal run-away.

There are at least three different contributions to the temperature dependence. The first is the thermal probability of finding a hopping conduction path through the material. Following Gerson and Marshall [7] and assuming a random isotropic distribution of traps, Scott [10] showed that

$$E_B = G - (k_B T/B) \log A, \tag{3}$$

which gives both the dependence on temperature T and electrode area A in agreement with practically all experiments on perovskite oxides (PZT, BST, and SBT). In the present work the electrode areas were typically 60 μm x 60 μm, and hence E_B might be larger (from Eq. (3)) than that in work elsewhere with larger electrodes but smaller than that obtainable with very small contacts of a few μm^2. This effect is independent of and in addition to any effects of Sm-doping. The range of electrode sizes in the present work did not permit a test of Eq. (3).

The further assumption of exponential conduction (non-ohmic):

$$\sigma(T) = \sigma_0 \exp[-\beta/k_B T] \tag{4}$$

estimated [11] to occur for applied field $E >$ 30 MV/m in these materials yields the correct dependence of breakdown time, t_B, upon field:

$$\log t_B = c_1 - c_2 E_B, \tag{5}$$

as well as the experimentally observed dependence of E_B on rise time t_c of the applied pulse:

$$E_B = c_3 \, t_c^{-1/2}. \tag{6}$$

Using the same assumption of exponential conduction, which is valid for

$$aeE << k_B T, \tag{7}$$

where a is the lattice nearest-neighbor oxygen-site hopping distance (approximately a lattice constant) and e, the electron charge, Scott shows [11] that the general breakdown field expression

$$C_V \, dT/dt - \nabla(K \cdot \nabla T) = \sigma E_B^2, \tag{8}$$

in the impulse approximation [in which second term in (8) is neglected] yields

$$E_B(T) = [3C_V K/\sigma_0 \beta t_c]^{1/2} \, T \exp[\beta/(2k_B T)] = \text{ca. 800 MV/m}, \tag{9}$$

for ceramic BST films and more recently in 70-nm thick single-crystal barium titanate. [12] However, in the present study of Sm-doped bismuth titanate, the breakdown field E_B averaged to be about 50 MV/m, an order of magnitude less than this theoretical estimate, due to the fact that the electrical conductivity coefficient σ_0 in Eq.(9) is larger by ca. 100 in bismuth titanate than in good BST films [E_B varies as $\sigma_0^{-1/2}$]. Note that in bismuth titanate, because the hopping distance a in Eq. (7) is very anisotropic (favoring conduction within Bi_2O_2-planes), the breakdown field is also expected to be anisotropic, unlike the cases of PZT or BST; this anisotropy is contained in Eq. (8), notably from the fact that the thermal conductivity K is a tensor, but it is neglected in the impulse approximation. Generally it results in an experimental breakdown field that is smaller than that predicted in the isotropic impulse approximation.

A controversy has arisen regarding the temperature dependence of $E_B(T)$ and the possibility of avalanche. [13] In low carrier concentration single crystals, especially Si, avalanche mechanisms give a temperature dependence that is controlled by the mean free path of the injected carriers. This is physically because at higher temperatures the mean free path λ decreases due to phonon scattering, and thus one must apply a higher field E_B to achieve avalanche conditions:

$$\lambda = \lambda_0 \tanh[E_g/(2k_B T)]. \tag{10}$$

However, this effect is extremely small even for low carrier concentrations (10% change in E_B between 300K and 500K for $n = 10^{16}$ cm^{-3}) and negligible for higher concentrations. The actual experimental change in E_B in BST between 600K and 200K is >500% and arises from T-dependence of other parameters Eq. (9), such as the activation energy β or the conductivity coefficient σ_0, not λ in Eq.(10). Even in single crystals any T-dependence from Eq.(10) would be immeasurably small; and for the actual 40-nm grain ceramics, the mean free path λ is ca. 1 nm (as follows from Eq.(2)) and limited by grain boundaries (T-independent). Thus the conclusion of Stolichnov *et al.* [13] regarding avalanche is unlikely in ferroelectric oxides.
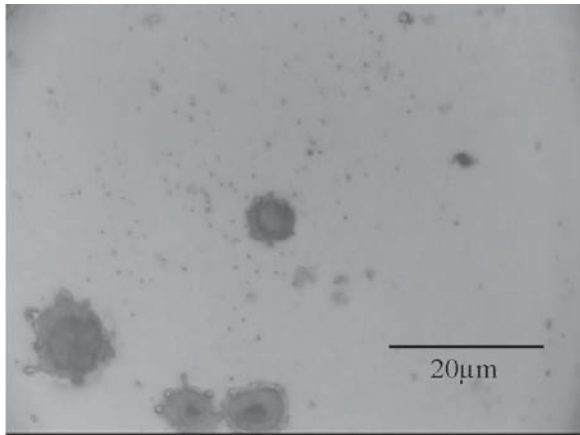
Fig. 1. Optical micrograph of fatigued region of PZT film; plan view showing cylindrical filamentary electrical shorts produced by excessive fatigue.

1.2. The role of bismuth

The considerations above tell us a lot about physical kinetics in ferroelectric breakdown but very little about the solid state chemical kinetics involved or the local crystal structure at the breakdown path. Nor do they suggest why breakdown might be different in different oxide ferroelectrics.

It is known that bismuth oxide (Bi_2O_3) phase separates under unexplained conditions, often related to film wetting, into metallic bismuth [14,15]. In bismuth-containing ferroelectric films such as bismuth titanate $Bi_4Ti_3O_{12}$ this can result in the self-assembly of partially registered arrays of islands of bismuth oxide [16]. It can also result in the loss of bismuth due to vaporization. The exact mechanisms of elemental Bi separation are unknown, but a possible cause in the case of sol-gel deposition is the presence of carbon impurities from the organics used as precursors; free C at the electrode-dielectric interface region will readily reduce bismuth oxides to metallic bismuth [17]. Very little is known about such phase separation processes in the strongly non-equilibrium conditions of electrical breakdown in thin films. Here we report phase separation of nominally pure bismuth titanate into phases which include pyrochlore. These thin films of samarium-bismuth titanate $Bi_{4-x}Sm_xTi_3O_{12}$ undergo a phase separation under conditions of electrical breakdown from a monoclinic (pseudo-orthorhombic) Pc-C_s^2 structure to a mix containing a fraction of pyrochlore structure $Bi_2Ti_2O_7$ (nominally P2$_1$-C_2^2) plus metallic bismuth, with a loss of oxygen and bismuth due to vaporization. In contrast with this, the breakdown of lead zirconate-titanate (PZT) appears to favor β-PbO

+ rutile and not a pyrochlore conversion. This is somewhat surprising since β-PbO is not the phase stable under ambient conditions and the perovskite-pyrochlore conversion is known to occur under purely thermal decomposition.

Tsang and Lindner have shown [18] that breakdown in oxide thin films consists of at least two stages, the first of which is reversible, and involve different behavior for n-type and p-type FETs. In the present work we complement their time dependence study of spatially localized hot carrier luminescence with micro-Raman studies of the chemical composition within micron-sized lateral areas of the filamentary breakdown paths.

2. EXPERIMENT

2.1. PZT

2.1.1. Preparation

Two compositions of sol-gel spin-coated PZT thin films have been used in present work: $PbZr_{0.3}Ti_{0.7}O_3$ with thickness d = 370 nm and $PbZr_{0.52}Ti_{0.48}O_3$ with thickness 540 nm.

2.1.2. Electrical breakdown

Our PZT films were shorted by fatiguing them with bipolar voltages of 21 V, 27 V, and 30 V until failure was achieved (>10^{11} cycles); these voltages correspond to a maximum of 80 MV/m and a minimum of 40 MV/m. The result was a number of filamentary shorts, typically < 10 microns in diameter. These are shown in Fig.1 as a [2D] map with the plan view illuminated by a 632 nm wavelength He-Ne laser and viewed through an optical microscope.

2.1.3. Micro-Raman spectroscopy

Within each dark circular spot we made a series of ca. 100 micro-Raman studies, which revealed phase-separated regions of lateral dimension ca. 1 micron or less. Raman studies used a Jobin-Yvon LabRam 300 with a 632.8 nm, 20-mW He-Ne laser backscattered from a 2 μm-diameter spot with CCD collection (10 minutes for 30 acquisitions). In order to survey the region between 150-200 cm^{-1}, we repeated the micro-Raman studies with a RM1000 Renishaw system and with a LabRam 300. As shown in Fig.2, these exhibited the spectra of easily identified PbO and rutile-phase TiO_2. We assign the sharp peak at 145 cm^{-1} and the peak at 338 cm^{-1} (B_{1g} mode) to the α-PbO phase, according to our own standard Raman spectra on PbO powders (unpublished), Adams' work [19] and the work of Hedous *et al.*
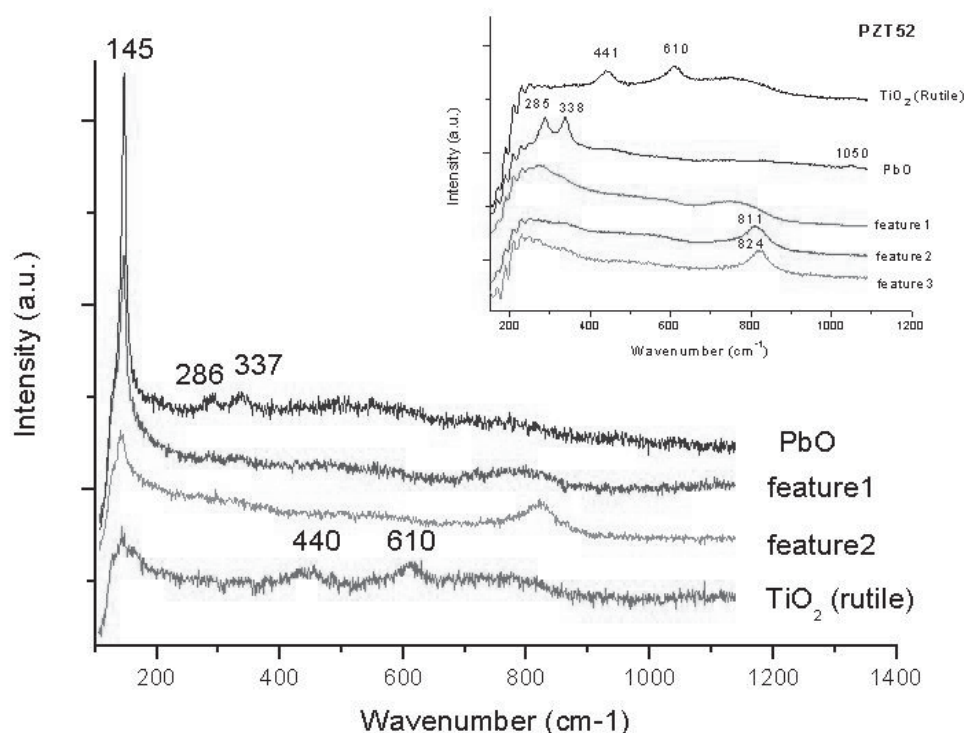
Fig. 2. Micro-Raman data of several 1 x 1 micron regions of the dark spots in the fatigued PZT film of Fig.1, showing distinct regions of PbO and TiO_2.

[20] The peak at 285 cm^{-1} is attributed to β-PbO [20]. Note that α-PbO is the only stable phase at ambient temperature and pressure. The high-pressure β-PbO may be stabilized at ambient conditions by surface strain due to the small size of the fatigued-induced PbO phase. Indeed, similar phase stabilization effects are well known in other oxide films, such as KNO_3. The ratio of the peak at 285 cm^{-1} and 338 cm^{-1} changes from spot to spot in our experiments, indicating their different properties and confirming our assignment. Additionally, γ-PbO$_2$ (medium-pressure phase) has peaks very close to those in α-PbO [19]. Therefore it is hard to tell the percentage of each PbO phase involved. We confidently assign the peaks at 140 cm^{-1}, 441 cm^{-1} and 610 cm^{-1} to the rutile phase of TiO_2 [21]. Other TiO_2 phases (i.e., brookite, anatase, *etc.*) have not been observed in our studies [22]. Note that although the rutile phase is well defined in the degraded (fatigued) PZT52 film, it has not been clearly observed in the fatigued PZT30 film. A thorough study by [2D] mapping is warranted on the PZT30 film. The small peak at 1050 cm^{-1} was frequently observed and the assignment is unknown so far. A detailed Raman study shows that the broad feature from 700 cm^{-1} to 900 cm^{-1} may contain three peaks/bands: (1) a broad band from 700 to 900 cm^{-1}, (2) a peak centred at 811 cm^{-1}, and (3) a peak centred 824 cm^{-1} (Fig. 2). We tentatively assign the broad band to Ti/Zr-O clusters, or possibly a pyrochlore phase, since this feature has also been observed during the annealing process of PZT thin films or powders [23,24]. We also note that Raman scattering study by Fu *et al.* shows that PbTiO$_3$ nano-crystals prepared by a sol-gel methods at 400 °C reveal a new phase (C_{4v} to C_{2v}) in the region near 166 °C when the size of the crystals decreases to 7 nm. The Raman spectra recorded from this new phase show similar features to those we observed at the degraded spots in our PZT films [25]. The peaks at 811 cm^{-1} and 824 cm^{-1} are attributed to well-ordered Ti-O clusters. The broadness of the general features indicates a rather amorphous structure.

2.1.4. Relationship to PZT pyrochlore studies

An interesting study was published by Camargo *et al.* [26]. The spectra they recorded from lead titanate powders calcined at 450 °C for 40 mins show a remarkably similarity to our fatigued PZT spectra (Fig. 2b in their paper). However, they (as well as

the references they cited) assigned all the features (145 cm^{-1}, 231 cm^{-1}, 285 cm^{-1}, 334 cm^{-1} and broad band at 741 cm^{-1}) to pyrochlore. Addtionally, a peak at 145 cm^{-1} has long been claimed to belong to a pyrochlore phase (see the work of Nomura *et al.* [24] and references therein). However, we assign these peaks at 145 cm^{-1}, 285 cm^{-1}, and 334 cm^{-1} as due to residue α/β-PbO during the annealing process, since our data show that the these three peaks definitely have no correspondence with the presence or absence of the broad band at 800 cm^{-1}. As the authors mentioned in their paper, the structure of the lead titanate formed at low temperatures is highly controversial. A definite conclusion is impossible at this stage, due to the lack of standard bench-mark spectra of the pyrochlore phase.

Another related topic is the decomposition of PZT at high temperatures; since micro-shorts produce local temperatures capable of melting or even vaporizing the PZT, this is pertinent. A very early work [27] by Castellano *et al.* indicated that 'the perovskite structure collapsed into the pyrochlore phase due to loss of oxygen when a sample deposited at 415 °C was heated to 800 °C for 10 min.' They also mentioned that the collapse of the perovskite structure is sensitive to oxygen vacancies (collapse at ca.15%) rather than lead vacancies, and that a large number of Pb vacancies do not lead to any structural changes. Additionally, Tabata *et al.* [28] reported that the pyrochlore-perovskite transformation occurs at 350-380 °C and a mixture of $PbTi_3O_7$ and TiO_2 exists above 550 °C. Chen and Chen reported a 'Pb-deficient pyrochlore-type phase of $PbTi_3O_7$' appearing at 800 °C when PbO rapidly evaporates [29]. However, this phase decomposition/separation has never been observed during electrical treatments - e.g., fatigue or breakdown. Our preliminary results show that the degradation in both fatigue and electrical breakdown is polarity independent. Micro-Raman techniques involve back-scattering geometries; the resulting stray light levels preclude obtaining phonon data below ca. 150 cm^{-1} that would be helpful in this regard.

2.2. Bismuth titanate

2.2.1. Preparation

Because of its fatigue-free behavior (P_r degrades only 5% at 100 °C after 10^{12} cycles in our work), samarium-doped bismuth titanate $Bi_{4-x}Sm_xTi_3O_{12}$ (BSmT, x~0.5) has strong commercial device potential and been chosen for study here; it has a multi-layered perovskite structure containing three perovskite-like blocks between two Bi_2O_3 sheets.
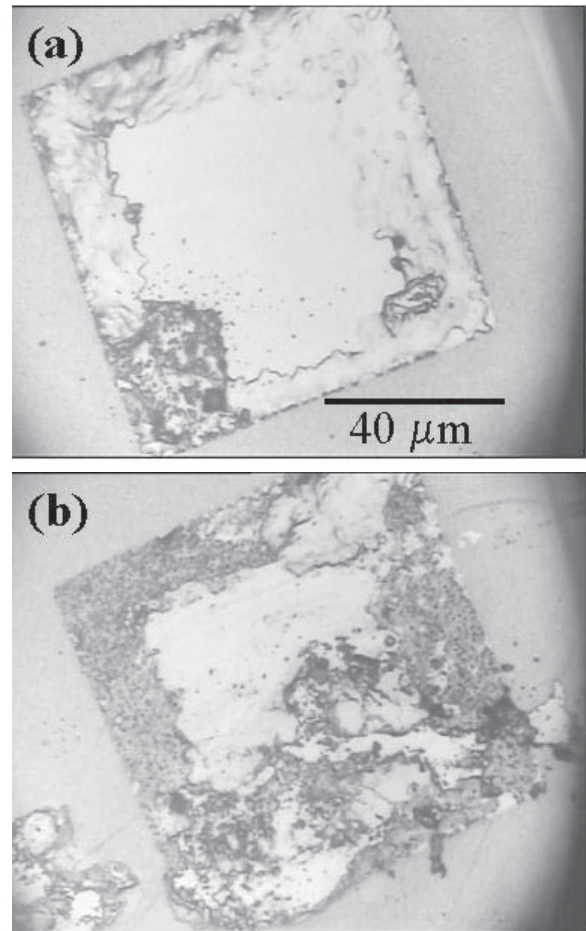

Fig. 3. Optical micrographs of: (a) the electroded surface (90 micron width Pt electrode) of Sm-doped bismuth titanate; (b) the underlying ferroelectric film showing shorted regions.

Films were fabricated by sol-gel spin-coating method on Pt/TiO$_2$/SiO$_2$/Si substrate, and were then annealed at 700 °C for 10 minutes in a flowing oxygen atmosphere.

2.2.2. Electrical breakdown

Because Sm-doped bismuth titanate is rather fatigue-free, it was not shorted by excessive fatigue, but instead by simply applying a field greater than the breakdown field.

The BSmT sample was shorted with a stepped dc voltage (0.2 V/step, 1 s/step) with maximum field $E > E_B$ (about 50 MV/m). By using a stepped voltage we could stop the shorting process after only a few shorts were produced, without extensive breakdown. However, even then the electrode was highly degraded (Fig. 3), especially at the edges (Fig. 3a). Raman scattering measurements were carried out on the film interface after electrode removal. Only
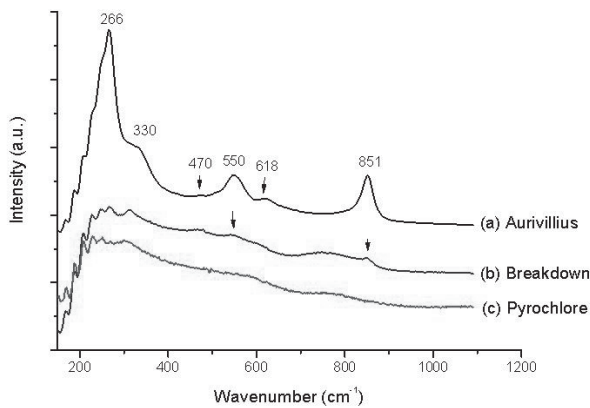
Fig. 4. Micro-Raman spectra of bismuth titanate films: (a) unshorted regions; (b) shorted regions; (c) undamaged film of known pyrochlore phase prepared by lower temperature (450 °C) anneal.

part of the film interfaces are degraded, as evidenced by randomly distributed multiple dark spots. The lighter green regions are the normal undamaged film, whereas the black regions are shorted or degraded.

2.2.3. Micro-Raman spectroscopy

Breakdown regions and the unaffected regions (showing phonon modes from the Aurivillius or layered-perovskite phase of the normal BSmT film [30]) are shown before and after breakdown, respectively, in Fig. 4a,b. The undamaged Aurivilius phase spectrum in 4a compares closely with that in [30]; in particular, for crossed polarizations the strongest line is at 267±2 cm^{-1}. A spectrum showing pyrochlore structure produced by us as a low-T anneal is also exhibited (Fig. 4c); it may be compared with those for pyrochlore and amorphous bismuth titanate structures in [31-34]. Raman data from the breakdown regions show almost identical features with the pyrochlore phase, collected from a BSmT sample prepared with the same deposition conditions, but annealed at a lower T = 450 °C. The three broad spectral peaks at ca. 280, 580, and 800 cm^{-1} agree rather well with those unambiguously established in pyrochlore-phase bismuth titanate [32].

2.2.4. Electron nano-probe results

In order to test this perovskite-pyrochlore hypothesis, elemental analysis has been conducted on different surface regions by assuming stoichiometric oxide conditions. SEM results are shown in Fig. 5 and summarized in Table 1. Pyrochlore phases

have formula $A_2B_2O_7$ with ionic ratio A/B ions of 1:1. The ionic ratio of ($Bi^{3+}+Sm^{3+}$) to Ti^{4+} is 4:3 (1.33) in the layered perovskite BSmT. From Table I, the A/B ratio is 1.37±0.02 for undamaged areas, and 1.21±0.02 for the breakdown region, compared with the ratio 1:1 expected for pyrochlore, showing that this region is about 50% converted. This is reasonable, because the nano-probe samples a region somewhat larger than the diameter of the filamentary breakdown, so that a Bi/Ti ratio somewhere between 1.33 and 1.00 is expected.

2.2.5. Relationship to fatigue studies

Güttler *et al.* first studied fatigue behaviour in PZT films by Raman and IR reflectance spectroscopy [35]. They argued that fatigue is accompanied by an increase of the Raman scattering intensities and mode hardening. They attributed the up-shift of these hard modes to the increased tetragonal distortion after fatigue. It is important to note in that the same kind of black spots arise on the surfaces of bismuth titanate films that are not intentionally shorted but are simply fatigued, as with the PZT films in Fig. 1. The insert in Fig. 5 shows the hysteresis measured in the regions free of nano-shorts. These dendritic paths of oxygen-deficient regions eventually produce microshorts [1]. Our analyses via electron nano-probe and Raman micro-probe show them also to be pyrochlore-rich. There has been a long-standing
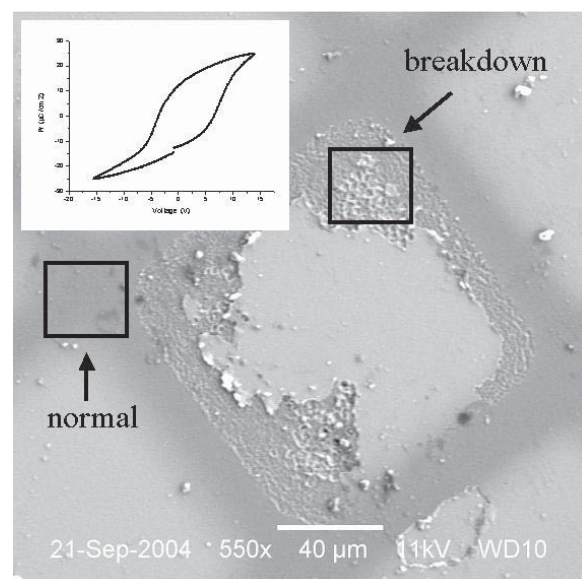

Fig. 5. Electron nano-probe (SEM) micrograph of the surface of a bismuth titanate film after dc breakdown. Insert: Hysteresis in this film before breakdown.

Table 1. SEM elemental analysis of shorted and unshorted regions 20 microns in width of the Sm-doped bismuth titanate film.

Element	Unshorted Region			Shorted Region		
	k-ratio	ZAF	at.%	*k*-ratio	ZAF	at.%
Bi-M	0.5531	1.155	18.5 ± 0.2	0.5430	1.160	17.7 ± 0.2
Ti-K	0.1330	0.925	15.5 ± 0.3	0.1459	0.931	16.6 ± 0.3
Sm-L	0.0617	1.148	2.9 ± 0.3	0.0531	1.158	2.4 ± 0.2

controversy as to whether oxygen atoms are actually lost during fatigue or merely redistributed [36]. We note that very similar results were reported very recently by Verdier, Lupascu *et al.* in bulk PZT, who found that after fatigue such damage could be etched or polished off the near-surface regions, restoring un-fatigued behavior [37].

3. SUMMARY AND CONCLUSIONS

A combination of micro-Raman spectroscopy and electron nano-probe data have been used to characterize phase separation in PZT and Sm-doped bismuth titanate films following electrical breakdown. In PZT the breakdown was caused by excessive electrical fatigue, whereas in the rather fatigue-free $Bi_4Ti_3O_{12}$:Sm, a stepped voltage was applied until breakdown threshold was reached. In each case phase separation in the filamentary shorts was measured quantitatively. The phase separation is quite different in PZT, where α- and β-phases of lead oxide and rutile result, from that in the Aurivilius-phase bismuth titanate, where neither B_2O_3 nor rutile is observed, but instead a pyrochlore-like phase depleted slightly in Bi. Ironically, the perovskite-pyrochlore decomposition is not a principle mechanism in PZT, where it might have been expected on the basis of earlier thermal decomposition studies. The α-β PbO phase boundary is [38] at only 400 °C at atmospheric pressure and only 4 kbar at room temperature, so that under the local pressures and temperatures of a relatively explosive electrical short, it might be anticipated that the β-phase is easily reached.

REFERENCES

[1] R. Plumlee // *Sandia Laboratories report* SC-RR-67-730 (1967).

[2] H. M. Duiker and P. D. Beale // *Phys. Rev*. **B41** (1990) 490.

[3] H. M. Duiker, Ph.D. thesis, Univ. Colorado (1990), available from University Microfilms (Ann Arbor, Mich.)

[4] H. M. Duiker *et al.* // *J. Appl. Phys*. **68** (1990) 5783.

[5] J. F. Scott, B. M. Melnick, L. D. McMillan and C. A. Paz de Araujo // *Integ. Ferroelec*. **3** (1993) 225.

[6] F. Forlani and N. Minnaja // *Phys. Stat. Sol*. **4** (1967) 311.

[7] R. Gerson and T. C. Marshall // *J. Appl. Phys*. **30** (1959) 1650.

[8] A. Von Hippel // *Z. Phys*. **98** (1936) 580; *J. Appl. Phys*. **8** (1937) 815.

[9] J. F. Scott // *Ferroelectric Memories* (Springer, Berlin, 2000), p.62; L. V. Zhoga, A. V. Shil'nikov, V. V. Shpeizman and G. G. Pankova // *Russian Phys. J.* **47** (2004) 172.

[10] J. F. Scott, In: *Science and Technology of Electroceramic Thin Films*, ed. by O. Aucilello and R. Waser, *Proceedings of the NATO Advanced Research Workshop* (Kluwer Academic, Dordrecht, 1995) p. 249.

[11] J. F. Scott // *Ferroelectric Memories* (Springer, Berlin, 2000) p.58.

[12] M. M. Saad, P. Baxter, R. M. Bowman, J. M. Gregg, F. D. Morrison and J. F. Scott // *J. Phys. Condens. Mat.* **16** (2004) L451.

[13] I. Stolichnov, A. Tagantsev, N. Setter, S. Okhonin, P. Fazan, J. S. Cross, M. Tsukada, A. Bartic and D. Wouters // *Integ. Ferroelec.* **32** (2001) 737.

[14] C. Rottman // *Scripta Metall.* **19** (1985) 43; A. J. Hartmann, R. Lamb, J. F. Scott, P. N. Johnston, M. El Bouanani, C. W. Chen and J. Robertson // *Proc. Korean Phys. Soc.* **32** (1998) S1329.

[15] B. E. Watts, F. Leccabue, G. Tallarida, S. Ferrari, M. Fanciulli and G. Padeletti //

Integ. Ferroelec. **62** (2004) 3; J. F. Scott,
M. Alexe, N. D. Zakharov, A. Pignolet,
C. Curran and D. Hesse // *Integ. Ferroelec.*
21 (1998) 14.

[16] M. Alexe, J. F. Scott, C. Curran, N. D.
Zakharov, D. Hesse and A. Pignolet // *Appl.
Phys. Lett.* **73** (1998) 1592; J. F. Scott, M.
Alexe, N. D. Zakharov, A. Pignolet, C. Curran
and D. Hesse // *Integ. Ferroelec*. **21** (1998)
1.

[17] C. A. Randall, private communication.

[18] J. C. Tsang and B. P. Lindner // *Appl. Phys.
Lett.* **84** (2004) 4641.

[19] D. M. Adams, A. G. Christy, J. Haines and
S. M. Clark // *Phys. Rev*. **B46** (1992) 11358.

[20] A. Hedoux *et al.* // *J. Phys. Condens. Mat*. **7**
(1995) 8547.

[21] P. Merle, J. Pascual, J. Camassel and
H. Mathieu // *Phys. Rev*. **B21** (1980) 1617.

[22] M. P. Moret, R. Zallen, D. P. Vijay and S. B.
Desu // *Thin Solid Films* **366** (2000) 8.

[23] J. Y. Fang, J. Wang, L. M. Gan and S. C. Ng
// *Mater. Lett*. **52** (2002) 304.

[24] K. Nomura, Y. Takeda, M. Maeda and
N. Shibata // *Jpn. J. Appl. Phys*. **39** (2000)
5247.

[25] D. S. Fu, H. Suzuki and K. Ishikawa // *Phys.
Rev*. **B62** (2000) 3125.

[26] E. R. Camargo, E. Longo, E. R. Leite and
V. R. Mastelaro // *J. Sol. St. Chem*. **177**
(2004) 1994.

[27] R. N. Castellano and L. G. Feinstein //
J. Appl. Phys. **50** (1979) 4406.

[28] H. Tabata *et al.* // *Appl. Phys. Lett*. **59** (1991)
2354.

[29] S. Y. Chen and I-W. Chen // *J. Appl. Phys*.
83 (1998) 7789.

[30] P. R. Graves, G. Hua, S. Myhra and J. G.
Thompson // *J. Sol. St. Chem*. **114** (1995)
112.

[31] N. Sugita, E. Tokumitsu, M. Osada and
M. Kakihana // *Jpn. J. Appl. Phys*. **42** (2003)
L944.

[32] N. Sugita, M. Osata and E. Tokumitsu // *Jpn.
J. Appl. Phys*. **41** (2002) 6810.

[33] D. Wu and A. Li // *J. Mater. Res.* **16** (2001)
1332.

[34] S. Kojima and A. Hushur // *J. Non-cryst.
Solids* **293** (2001) 250.

[35] B. Guttler, U. Bismayer, P. Groves and
E. Salje // *Semiconduct. Sci. & Tech*. **10**
(1995) 245.

[36] M. Dawber and J. F. Scott // *Appl. Phys.
Lett*. **76** (2000) 3801.

[37] C. Verdier, F. D. Morrison, D. Lupascu and
J. F. Scott // *J. Appl. Phys*. **97** (2005)
024107.

[38] R. C. Keezer, D. L. Bowman and J. H.
Becker // *J. Appl. Phys*. **39** (1968) 2062.